PROCEEDINGS, 1st International Workshop on WATER DYNAMICS
Tohoku University, Sendai, Japan, 17-19 March, 2004

Synthesis of water-soluble fullerenes and their characterization

Y. AKIMOTO[1], K.SHINODA[1], B. JEYADEVAN[1], K. TOHJI[1], K. KAYA[1], T. MATSUMOTO[2], M. WAELCHLI[3], Y. KURODA[3]

1. Graduate School of Environmental Studies, Tohoku University, Sendai, Japan
2. Institute of Multidisciplinary Research for Advanced Materials, Tohoku University, Sendai, Japan
3. Bruker Biospin CO. LTD., Tsukuba, Japan

We report a new and simple method to synthesize water-soluble fullerenes. Here, the fullerene oxides are simply boiled in alkali aqueous solution to obtain water-soluble species. The mass analysis of water-soluble sample confirms the presence of C_{60} suggesting the dissolution of the same in water. Furthermore, the structure of the water-soluble fullerenes was analyzed in detail by using the Fourier transform infrared, ultraviolet- visible analysis and NMR. We expected to arrive at the structure of the water-soluble fullerenes that has the composition of $C_{60}H_{2n}(OH)_{2n}$ from these analyses.

1. Introduction

Water-soluble fullerene derivatives have a great potential in the field of biological and medical applications. For example, C_{60} derivatives have been applied as anti-HIV and anti-cancer reagents. Chiang et al. and Kitazawa et al. have succeeded in producing water-soluble fullerene, $C_{60}(OH)_n$ using two different methods developed separately. Chiang et al. synthesized the water-soluble fullerene by the hydrolysis of ester moieties of a polyorganocarboxylated fullerene derivative "L.Y.Chiang et al (1992) found". On the other hand, Kitazawa et al. reported a more efficient reaction between C_{60} and NaOH aq, and used tetrabutylammonium hydroxide as phase transfer catalyst "K.Kitazawa et al (1993) found". However, the above methods required numerous steps and several reagents and also had some ions associated in the final products, which hampered their use directly. Therefore, we suggest a simple and efficient method to synthesize water-soluble fullerenes utilizing the fullerene oxides and nucleophilic addition.

2. Experiment

C_{60} was overoxidized by bubbling with ozone gas in C_{60} toluene solution. This treatment was continued until the precipitate was formed (about 20 minutes). Then, the precipitate was filtered and dried. Water-soluble fullerene derivatives were synthesized by boiling the precipitate in NaOH aqueous solution. Then, the suspension was filtered to remove insoluble species. The filtrate was treated with ion-exchange resin to remove sodium ions present in the solution and analyzed by MALDI-TOF-MS (Bruker, Reflex III), FT-IR (Thermo Nicolet, AVATAR360), ultraviolet-visible spectrophotometer (HITACHI, U-3300), and ^{13}C-, ^{1}H-NMR (Bruker, Cryoprobe AV500). Then, MM calculation was used to predict the orientation of the functional group of fullerene.

3. Results and Discussion

Figure 1 shows the result of the mass analysis of the synthesized water-soluble fullerene. The matrix used 2.5-dihydroxy benzoic acid. In the mass spectrum, the peak of only C_{60} was observed. Therefore, the determination of the number of functional groups in a fullerene is not possible. However, it is expected that water-soluble fullerene derivative retains fullerene cage.

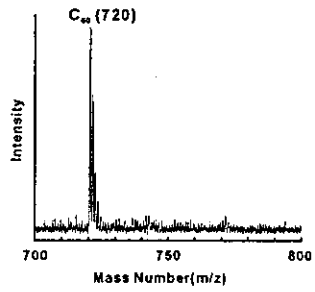

Fig1. Mass spectrum of water-soluble fullerene.

Figure 2 shows the results of IR and UV-vis analysis of water-soluble fullerene. In the IR spectrum, absorption bands corresponding to C-O(1200~1000 cm^{-1}), C-H(about 2900cm^{-1} and 1400cm^{-1}), C=O(about 1700cm^{-1}) and

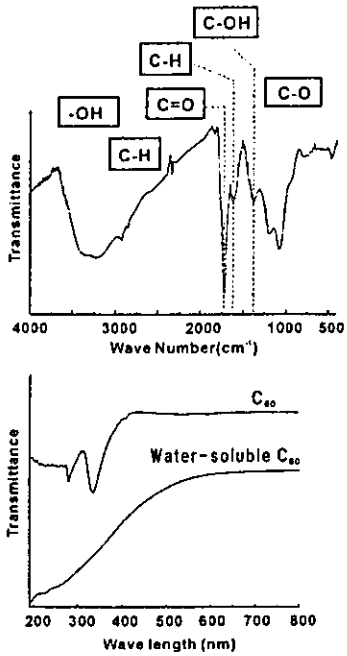

Fig2. IR and UV-vis spectra of water-soluble fullerene

hydroxyl(about 3400cm^{-1} and 1600cm^{-1}) were observed. However, the absorption bands of C_{60} were not observed at all. And also, in the UV-vis spectrum of water-soluble fullerene, the specific absorption band of C_{60} was not observed. The spectrum was broad. It could be expected that this is due to the hydroxyl absorption, which would have drastically changed the natural bonding states of C_{60}.

Figure 3 shows the results of ^{13}C-NMR and ^{1}H-NMR. The ^{13}C-NMR spectrum in D_2O exhibited two signals at about 173, 135 ppm for sp^2 carbons and three signals at about 62, 51 and 33 ppm for sp^3 carbons. The number of peaks in the ^{13}C-NMR spectrum is small. Thus, it is considered that the water-soluble fullerenes have a good structural symmetry. The ^{1}H-NMR spectrum in D_2O exhibited three signals at 4.7, 3.24 and 2.11 ppm. The 4.7 ppm peak is identified with water. The structures expected from the peaks of 2.11 and 3.24 ppm are H-C-C-OH and C-C-(H,OH). The structure of the water-soluble fullerene was considered as follows.

(1) The parts of 6-6 bonds of fullerene are broken.
(2) The functional groups such as proton (-H) and hydroxyl (-OH) ion are attached to the carbon atom in fullerene.
(3) The fullerene derivatives have the composition of $C_{60}H_{2n}(OH)_{2n}$.

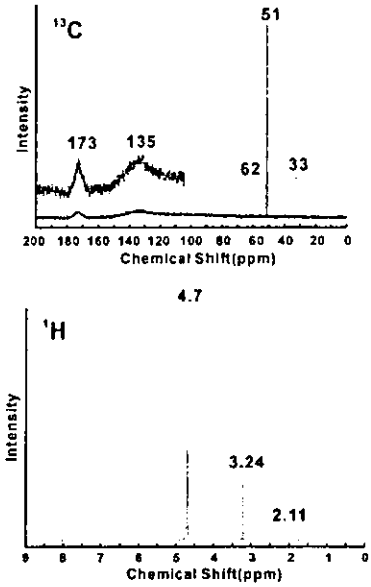

Fig3. ^{13}C- and ^{1}H-NMR spectra of water-soluble fullerene.

Figure 4 shows the optimum model of the water-soluble fullerene, which was calculated by MM. From the results of this calculation, the structure with hydroxyls attached to the symmetrically opposite positions is found to be the stablest.

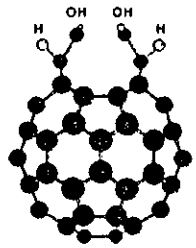

Fig4. The structure expected from MM calculation.

4. Conclusions

The water-soluble fullerene was synthesized by using the fullerene oxides and utilizing the nucleophilic addition reaction. The fullerene derivative with the above unique structure is yet to be reported. Thus we could conclude that we have succeeded in the synthesis of novel fullerene derivative.

References

J.Li, A.Takeuchi, M.Ozawa, X.Li, K.Saigo, K.Kitazawa, *J.Chem.Commun.*, 1993, p.1784

L.Y.Chiang, R.B.Upasani and J.W.Swirczewski, *J. Am.Chem.Soc.*, 1992, 114, 10154

PROCEEDINGS, 1st International Workshop on WATER DYNAMICS
Tohoku University, Sendai, Japan, 17-19 March, 2004

SYNTHESIS OF FERRITE NANOPARTICLES THROUGH AQUEOUS PROCESS FOR BIOMEDICAL APPLICATIONS

R. JUSTIN JOSEYPHUS[1,2], C. N. CHINNASAMY[1], B. JEYADEVAN[1], A. KASUYA[3], K. SHINODA[1], A. NARAYANASAMY[1,2,3], K. TOHJI[1]

[1]Graduate School of Environmental Studies, Tohoku University, Aoba-ku, Sendai 980-8579, Japan
[2]Materials Science Centre, Department of Nuclear Physics, University of Madras, Chennai 600 025, India
[3]Center for Interdisciplinary Research, Tohoku University, Sendai 980-8578, Japan

SUMMARY - The magnetic properties of materials deteriorate when the particle size reaches the superparamagnetic limit and hence it is important to have an appropriate particle size depending on the end use. In this paper we describe the synthesis of manganese zinc ferrite through aqueous process. Oxidation method has been employed through acqueous process to achieve large particles with high magnetization at low temperatures compared to other chemical methods. The synthesis conditions have been optimized to maximize the magnetization by increasing the particle size above the superparamagnetic threshold. The optimum concentration of the oxidant required for ferrite synthesis has been found to be 0.08 M of KNO_3 for 0.5 M NaOH. The results show that the largest particle size that could be achieved using the oxidation method is 80 nm and the magnetization is 49 Am^2/kg.

1. INTRODUCTION

Ferrite nanoparticles find important applications in high frequency devices, information storage, heat transfer devices, drug delivery systems and medical diagnostics. Nanosize particles of ferrites can be prepared by using various synthesis techniques namely ball-milling, citrate precursor method, hydrothermal synthesis, coprecipitation and oxidation methods. Mangenese zinc ferrites are useful for ferrofluid and biomedical applications due to low Curie temperature and high magnetization-temperature gradient. The magnetization value depends on the particle size as smaller particle size leads to superparamagnetism and decreases the magnetization.

In order to increase the magnetization the particle size has to be increased. Synthesis of ferrites through ball milling results in agglomerated particles and other methods like hydrothermal method involve high temperatures. Coprecipitation method results in smaller particle size and hence the magnetization value is low since the particle sizes are of the order of 10-20 nanometer and their magnetic properties are also influenced by parameters like cation distribution "Jeyadevan et al (2000)". Oxidation method can be used to synthesise nanoparticles of bigger sizes compared to the coprecipitation technique. However, the largest particle size obtainable with the oxidation method also varies according to the synthesis conditions used. In this paper we describe the synthesis of Mn-Zn ferrite through oxidation method involving low temperature synthesis in an aqueous medium and its magnetic properties with respect to particle size.

2. MATERIALS AND METHODS

Mn-$ZnFe_2O_4$ was synthesized using analytical grade reagents of $Fe_2SO_4.7H_2O$, $MnCl_2.4H_2O$, $ZnSO_4.H_2O$ and adopting the oxidation method. The ratio of Mn^{2+} to Zn^{2+} ions was fixed as 2 for all the experiments. NaOH was used for precipitation and KNO_3 was used as the oxidant. All the chemicals were of purity greater than 99% (Wako). Oxidation method can be used to synthesize larger particles by oxidising the hydoroxide precipitate with an oxidant to convert the ferrous ions to ferric and form the ferrite phase at lower temperatures. Fe, Mn and Zn salts were dissolved separately in water (0.5 L) and allowed to react with NaOH dissolved in the same amount of water. The resulting precipitate was purged with N_2 before heating to prevent atmospheric oxidation. The metal hydroxide precipitate with a pH between 12-13 was oxidized with various amounts of KNO_3 in a water bath at 90 °C with constant mechanical stirring. The duration of the reaction was 2 h. The phases produced were analyzed using X-ray diffraction (XRD). The average grain size was determined using the Scherrer formula. The morphology of the particles was examined using Scanning Electron Microscopy (SEM). The magnetic properties were measured using a Vibrating Sample Magnetometer (VSM).

The basic reaction mechanism of ferrite formation in the simple case of $FeO.Fe_2O_3$ (magnetite) is as follows:

(a) Fe(II) hydrolysis:

$Fe^{2+} + H_2O \rightarrow FeOH^+ + H^+$

(b) Fe(II) oxidation:

$2FeOH^{+} + 1/2\ O_2 + H_2O \rightarrow 2\ Fe(OH)_2^{+}$

(c) Precipitaion of partially oxidized intermediate:

$(2\text{-}x)Fe(OH)_2^{+} + (1+x)Fe(OH)^{+} + xSO_4^{2-} + (3\text{-}2x)OH^{-} \rightarrow (Fe^{3+})_{2-x}(Fe^{2+})_{1+x}(SO_4^{2-})_x(OH^{-})_{8-3x}$

(d) Additional Fe(II) oxidation at constant pH:

$2[(Fe^{3+})_{2-x}(Fe^{2+})_{1+x}(SO_4^{2-})_x(OH^{-})_{8-3x}] + x/2\ O_2 + 5xH_2O \rightarrow 2\ [(Fe^{3+})_{2-x}(Fe^{2+})(OH^{-})_8] + 2xH_2SO_4$

(e) De-hydration and magnetite formation:

$[(Fe^{3+})_{2-x}(Fe^{2+})(OH^{-})_8] \rightarrow FeO.Fe_2O_3 + 4H_2O$

From these reactions, it is seen that the ferrite phase formation occurs by hydrolysis and subsequent dehydration. A similar reaction mechanism takes place in the synthesis of Mn-Zn ferrite also. The ferrite phase formation also depends on the temperature and duration of the reaction. In the case of Mn-Zn ferrites, the temperature of 90 °C and the duration of 2 h were sufficient for the reaction to complete.

Metal salts of 0.17 M are allowed to react with 0.5 M of NaOH. The resulting metal hydroxide precipitate was heated with various moles of KNO_3. The KNO_3 mole values used were 0.05 M, 0.07 M, 0.08 M, 0.09 M, 0.15 M and 0.20 M.

3. RESULTS AND DISCUSSION

Fig.1 shows the XRD of the Mn-$ZnFe_2O_4$ sample with (a) 0.08 M (b) 0.09 M and (c) 0.20 M. The XRD showed the formation of pure spinel phase with increasing moles of KNO_3. The average grain size was found to be in the range of 23-27 nm upto 0.09 M KNO_3 and thereafter decreased to

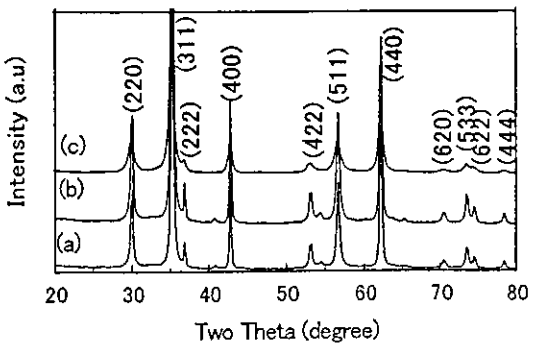

Fig.1. The XRD of the Mn-$ZnFe_2O_4$ sample with KNO_3 of (a) 0.08 M, (b) 0.09 M and (c) 0.20 M.

12 nm for the 0.20 M KNO_3 sample. For the lowest concentration of KNO_3 a small amount of hydroxide impurity peak is observed. Fig.2 shows the SEM photographs of the 0.09 M KNO_3 added sample. It is seen from the SEM results that the average particle size is 80 nm for the samples synthesized with less than 0.09 M of KNO_3 and

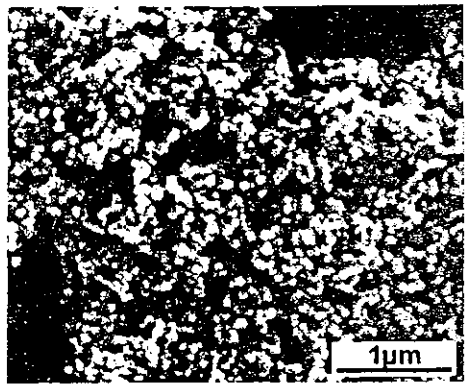

Fig.2. The SEM photograph of the Mn-$ZnFe_2O_4$ synthesized with 0.09 M KNO_3.

the average particle size decreased to less than 20 nm when the KNO_3 was 0.20 M. Fig.3 shows the saturation magnetization as a function of KNO_3 concentration. It is seen that the saturation magnetization is maximum with 49 Am^2/kg for the 0.08 M sample whereas it decreases to 39 Am^2/kg for the 0.20 M of KNO_3 due to reduction of particle size. The Mn-Zn ferrite particles synthesized using coprecipitation method have

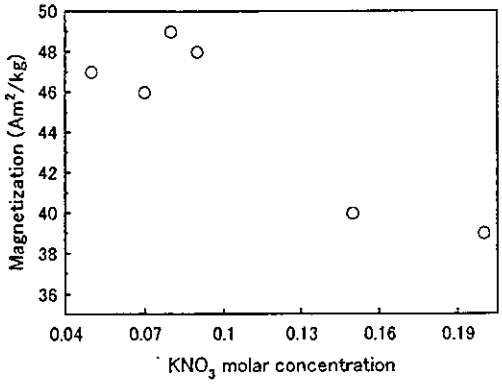

Fig.3. The saturation magnetization of the Mn-$ZnFe_2O_4$ as a function of KNO_3 concentration.

given a magnetization value of 37 Am^2/kg for 9 nm particles as reported by "Jeyadevan *et al* (2003)" whereas with the oxidation method we are able to synthesise 80 nm nanoparticles with a magnetization of 49 Am^2/kg.

4. CONCLUSIONS

Mn-Zn ferrite has been prepared by the oxidation method. The spinel phase formation depends upon the concentration of the oxidant used and the optimum amount of KNO_3 required for the maximum particle size is found to be 0.08 M for a fixed molar concentration of metal salts. The largest magnetization obtained is 49 Am^2/kg for a particle size of 80 nm.

5. ACKNOWLEDGEMENTS

This study was supported by grant-in-aid for basic research B#15360003 from the Ministry of Education, Science, Culture and Sport of Japan.

6. REFERENCES

Jeyadevan, B., Tohji, K., Nakatsuka, K., and Narayanasamy, A. (2000). Irregular distribution of metal ions in ferrites prepared by co-precipitation technique structure analysis of Mn–Zn ferrite using extended X-ray absorption fine structure. *J. Magn. Magn. Mater.*, Vol.217, 99-105.

Jeyadevan, B., Chinnasamy, C. N., Shinoda, K., Tohji, K., and Oka, H. (2003). Mn-Zn ferrite with higher magnetization for temperature sensitive magnetic fluid. *J. Appl. Phys.*, Vol.93, 8450-8452.

Appl. Phys. A 79, 85–87 (2004)
DOI: 10.1007/s00339-004-2599-9

Applied Physics A
Materials Science & Processing

Rapid communication

G.-H. JEONG[1,✉]
N. SATAKE[1]
T. KATO[1]
T. HIRATA[1]
R. HATAKEYAMA[1]
K. TOHJI[2]

Simple methods for site-controlled carbon nanotube growth using radio-frequency plasma-enhanced chemical vapor deposition

[1] Department of Electronic Engineering, Tohoku University, Sendai 980-8579, Japan
[2] Department of Geoscience and Technology, Tohoku University, Sendai 980-8579, Japan

Received: 14 July 2003/Accepted: 15 January 2004
Published online: 27 February 2004 •

ABSTRACT We demonstrate the validity of very simple methods for site-controlled carbon nanotube growth using a radio-frequency magnetron-type plasma-enhanced chemical vapor deposition technique. Enhanced plasma density and optimized ion-bombardment energy achieved by magnetic field introduction are found to be responsible for the uniform and well-aligned carbon nanotube growth. Based on these results, we attempted to perform experiments on site-controlled carbon nanotube growth using very convenient methods such as scratching or simply masking a substrate surface where carbonaceous materials deposit.

PACS 61.46.+w; 52.80.Pi; 81.15.Gh

1 Introduction

Because of their unique and prominent properties, carbon nanotubes have attracted a great deal of attention both scientifically and industrially. Especially, extensive studies have focused on the development of simple and controlled nanotube growth techniques for the purpose of industrial applications to various fields [1]. Concerning the site-selective growth, numerous techniques such as electron-beam lithography [2], a template method using porous materials [3], and ion-beam surface treatment [4] have been reported so far. When we use electron-beam lithography or the template method, which have been regarded as the representative techniques to prepare catalytic arrays, multi-walled carbon nanotubes (MWNTs) are generally produced in a highly site-controlled manner. However, their growth is limited to a very small area (in the case of the lithography technique) or involves following some cumbersome processes (in the case of the template method) such as wet etching and cleaning. On account of the relatively easy control of ion-bombardment energy and ion flux toward growing nanotubes, on the other hand, plasma-enhanced chemical vapor deposition (PECVD) has extensively been used for the individual and vertically aligned growth of the MWNTs in relation to their potential applications mainly as an electron emitter [5]. Here, we demonstrate very simple methods for the site-controlled MWNT growth in a quite large area using a radio-frequency PECVD (rf-PECVD) technique.

2 Experimental

In order to construct an rf (13.56 MHz) magnetron-type plasma apparatus, a magnetic field ($0 \leq B_z \leq 340$ G) is externally imposed parallel to a cylindrical rf electrode (3 cm in diameter) using solenoid coils [6]. Different from the prevailing parallel-plate PECVD units, the cylindrical rf electrode is made of Ni and surrounded by a grounded cylindrical chamber (13 cm in inner diameter and 30-cm long). This unique geometry gives rise to lower plasma sheath voltages at the rf electrode and higher plasma densities, which may endow optimal growth conditions. Essential plasma parameters such as plasma density n_e, electron temperature T_e, and plasma potential φ_p are measured by a Langmuir probe.

Figure 1a shows the effect of gas pressures on the radial profile of plasma density with $B_z = 170$ G. It is found that

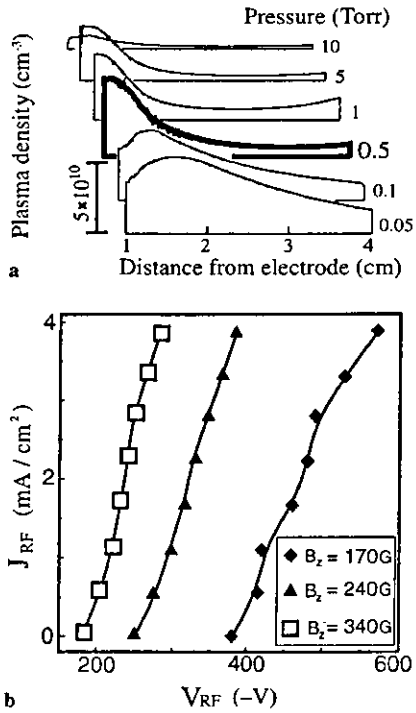

FIGURE 1 **a** Plasma density profiles in a radial direction for various gas pressures, **b** relationships between J_{rf} and V_{rf} for typical magnetic field strengths

✉ Fax: +81-22/263-9375, E-mail: hatak17@ec.ecei.tohoku.ac.jp

the plasma density is enhanced in the vicinity of the rf electrode and reaches a maximum when the working pressure is 0.5 Torr. It is to be noted that the product of electron-cyclotron frequency (ω_{ce}) by electron-neutral collision time (τ_{en}) is of the order of $\omega_{ce}\,\tau_{en} = 1$ under these conditions, which is an important quantity in magnetic confinement of plasmas. In addition to this, the dc voltage component (V_{rf}) of and the dc current density (J_{rf}) toward the rf electrode can be externally controlled as presented in Fig. 1b by connecting a dc power supply to it through a low-pass-filter circuit.

As a pretreatment [7], Ar sputtering has been performed for 15 min with the rf power of 1 kW. After this, a 15-min glow discharge (1-kW rf power, $CH_4 : H_2 = 9 : 1$) gives rise to vertically grown MWNTs on the powered rf-electrode surface. Field-emission scanning electron microscopy (FE-SEM, Hitachi S-4100) and field-emission transmission electron microscopy (FE-TEM, Hitachi HF-2000) are mainly employed to characterize the features of the carbon nanotubes grown.

3 Results and discussion

Firstly, according to Fig. 2a showing the feature of MWNTs grown for 3 min, it is observed that the MWNTs start to grow from, mainly, the top of protruding nano-islands (see inset) with various diameters. Thus, these islands formed by Ar plasma treatment are considered to play an important role in the nanotube formation, particularly at the primitive stage of the nanotube formation. Although carbon nanotube tip-growth mechanisms, which are commonly observed in the case of PECVD and explained in terms of surface adsorption on the catalyst, decomposition, diffusion, and final precipitation of carbon species in the form of a honeycomb structure, are frequently predicted in the literature [1, 8, 9], the specific investigation of the nucleation stage has almost never been reported. Very recently, we have reported the time evolution of the nucleation and further vertical growth using the PECVD method and found that the nanotube nucleation process firstly takes place through the catalyst tip formation preferentially from the protruding nano-islands due to an enhanced sputtering effect by the electric field concentration at the topmost region of the nano-islands, as shown in the inset of Fig. 2a [10].

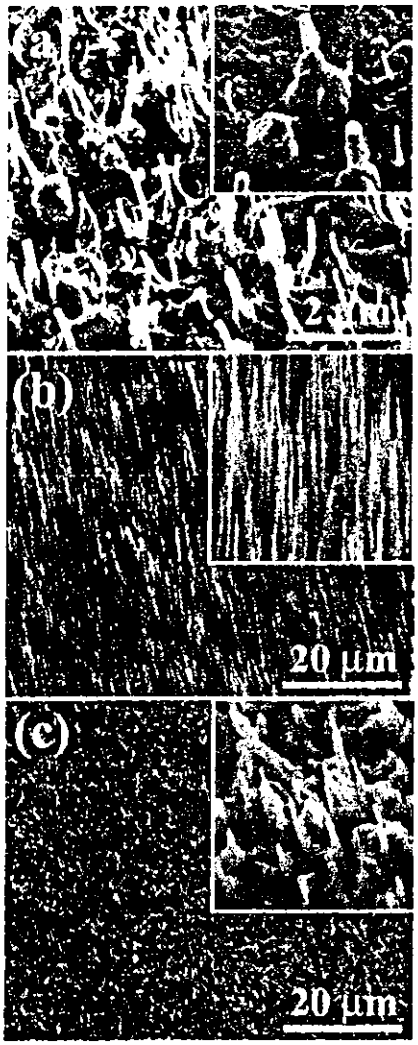

FIGURE 2 FE-SEM images. **a** After 3-min nanotube growth, **b** uniform and well-aligned MWNTs, **c** MWNT structure damaged by plasma ion bombardment

In order to investigate effects of magnetic field in our magnetron-type rf-PECVD, the dc component of the rf electrode, V_{rf}, is externally changed for typical magnetic fields (170 and 340 G) under the conditions of 0.5 Torr, $CH_4 : H_2 = 9 : 1$, and the rf power of 1000 W for 15 min. As we can see in Fig. 2b, uniform, dense, and well-aligned MWNTs grow in the externally biased case of $J_{rf} = 1.5\ \mathrm{mA/cm^2}$, $V_{rf} = -235$ V. On the other hand, when V_{rf} becomes extremely low, which is accompanied with an increase of ion flux ($J_{rf} = 4.0\ \mathrm{mA/cm^2}$, $V_{rf} = -570$ V), the nanotubes once formed are damaged due to a sputtering effect by both the high ion-bombardment energy and a surplus of ion flux from the plasma, as shown in Fig. 2c. From this result, it is clearly indicated that not merely ion flux, J_{rf}, but also ion-bombardment energy, V_{rf}, has to be optimized for the dense and well-aligned nanotube growth.

As explained above, the PECVD method is advantageous to controlled nanotube growth because the configuration and structure of resultant nanotubes grown can be varied by controlling the ion flux and the bombardment energy, which has not seen in any other nanotube formation methods. Utilizing this versatility of the PECVD method, we attempt to control the nanotube growth site in a simple way. Before inducing the mixture-gas discharge, the polished Ni surface was scratched linearly using a commercial sandpaper. After that, the mixture gas is discharged without the plasma pretreatment under the same condition of Fig. 2b. Figure 3 shows a FE-SEM image of MWNTs which are produced in the form of a linear array in this case. When the Ni surface is scratched, linearly arrayed projections are formed along both sides of the scratch line. Since these projections are considered to play the same role as the nano-islands in Fig. 2a, vertically well-aligned MWNTs are finally produced in a controlled manner.

On the other hand, we also attempt to produce the MWNTs in a large and selected area under the similar condition of Fig. 2c. In this situation, a region

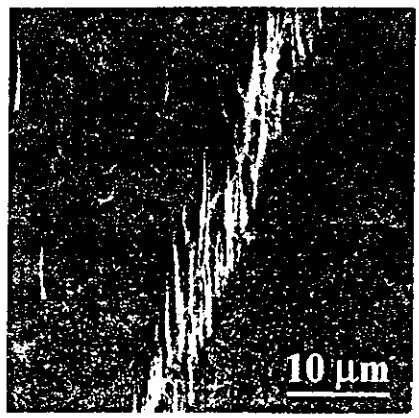

FIGURE 3 FE-SEM image showing the linearly arrayed MWNTs grown in the case of using the scratching method

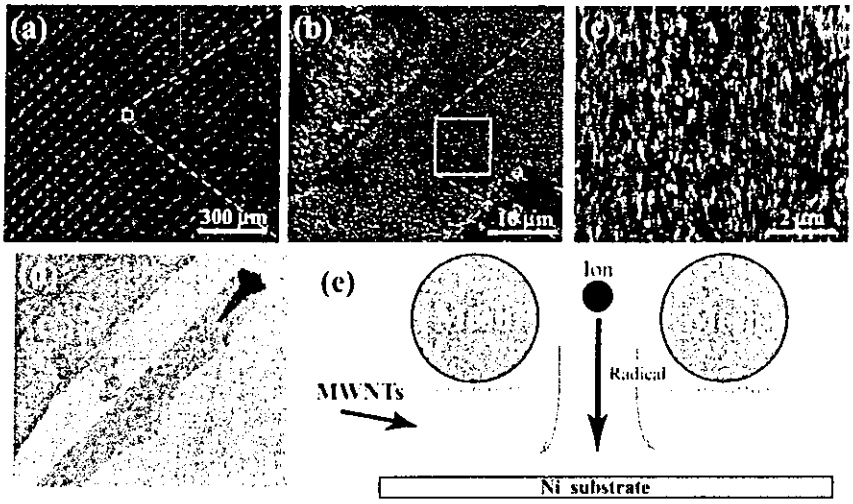

FIGURE 4 a, b, and c FE-SEM images showing the site-selectively grown MWNTs in a large area; the rectangular regions marked by *dotted lines* in (a) and (b) correspond to the images of (b) and (c), respectively, d FE-TEM image of an individual MWNT, e schematic illustration of the proposed model

of the rf-electrode surface, which is exposed to the plasma, is baneful to the vertical growth due to the intensive sputtering. Here, we introduce a commercial mesh in order to wrap a surface of a Ni substrate attached onto the rf electrode and therefore mask it to avoid the harmful sputtering phenomenon.

FE-SEM images in Fig. 4 show that the MWNTs are distributed with a high uniformity in a large area (see, in particular, Fig. 4a) and their location strongly supports the site-controllability (Fig. 4b and c). It is found that the MWNTs are formed beneath the mesh with a high density and a growth rate of 0.1 μm/min. On the contrary, it is hard to confirm the existence of MWNTs grown in the plasma-exposed regions, which is due to the direct sputtering of the high-energy positive ions, as already mentioned. A FE-TEM image of the individual MWNT in the same sample is given in Fig. 4d and reveals that the nanotube growth proceeds by the tip-growth mechanism because the Ni catalyst appears at the tube apex. Based on these results of the direct observations, a simple model describing the real situation is schematically illustrated as presented in Fig. 4e. In this study, it is conceived that MWNT growth characteristics beneath the mesh are similar to those of the thermal CVD rather than the usual PECVD because the Ni substrate surface is heated to ~ 650 °C by plasma ion bombardment and the affluent carbonaceous species such as CH_x radicals are supplied from the localized plasma state by the magnetic field introduction. It is an undeniable fact that these methods introduced here might not be superior to the electron-beam lithographic patterning or template technique in a sense of the precise site control. However, in the case of carrying out coarse patterning in a large area, our methods have the obvious advantage that we only need the really simple process, scratching or masking a plate. In addition, although our cylindrical PECVD system can not be directly applied to prevailing flat substrates, it is very helpful to apply it to a light source with a cylindrical geometry [11]. Moreover, if further detailed investigations are performed regarding the electric field concentration effect in the nanoscale, the selectivity in our methods is expected to be improved.

4 Conclusions

In summary, we have investigated the optimal plasma condition for the well-aligned MWNT growth and attempted to produce MWNTs in an easy manner with site-controlled growth using a cylindrical rf magnetron-type PECVD unit. It is found that the ion flux and the ion-bombardment energy have to be optimized in order to grow uniform, well-aligned, and density-controlled nanotubes. In a series of experiments it is finally demonstrated that very simple methods basically making use of the ion-bombardment energy are effective and available in a wide sense for the site-controlled carbon nanotube growth

ACKNOWLEDGEMENTS The authors thank K. Motomiya for his technical support. Part of this work was carried out under the Cooperative Research Project Program of the Research Institute of Electrical Communication, Tohoku University. This work was also supported by a Grant-in-Aid for Scientific Research from the Ministry of Education, Culture, Sports, Science and Technology, Japan.

REFERENCES

1 M. Meyyappan, L. Delzeit, A. Cassell, D. Hash: Plasma Sources Sci. Technol. **12**, 205 (2003)
2 V.I. Merkulov, D.H. Lowndes, Y.Y. Wei, G. Eres, E. Voelkl: Appl. Phys. Lett. **76**, 3555 (2001)
3 S. Fan, M.G. Chapline, N.R. Franklin, T.W. Tombler, A.M. Cassell, H. Dai: Science **283**, 512 (1999)
4 A. Gohel, K.C. Chin, K.Y. Lim, S.T. Tay, R. Liu, G.S. Chen, A.T.S. Wee: Chem. Phys. Lett. **371**, 131 (2003)
5 G. Pirio, P. Legagneux, D. Pribat, K.B.K. Teo, M. Chhowalla, G.A.J. Amaratunga, W.I. Milne: Nanotechnology **13**, 1 (2002)
6 N. Satake, G.-H. Jeong, T. Hirata, R. Hatakeyama, H. Ishida, K. Tohji, K. Motomiya: Physica B **323**, 290 (2002)
7 Z.F. Ren, Z.P. Huang, J.W. Xu, J.H. Wang, P. Bush, M.P. Siegal, P.N. Provencoi: Science **282**, 1105 (1998)
8 T. Hirao, K. Ito, H. Furuta, Y.K. Yap, T. Ikino, S. Honda, Y. Mori, T. Sasaki, K. Oura: Jpn. J. Appl. Phys. **40**, L631 (2001)
9 Y.S. Woo, I.T. Han, Y.J. Park, H.J. Kim, J.E. Jung, N.S. Lee, D.Y. Jeong, J.M. Kim: Jpn. J. Appl. Phys. **42**, 1410 (2003)
10 T. Hirata, N. Satake, G.-H. Jeong, T. Kato, R. Hatakeyama, K. Motomiya, K. Tohji: Appl. Phys. Lett. **83**, 1119 (2003)
11 J.M. Bonard, T. Stöckli, O. Noury, A. Châtelain: Appl. Phys. Lett. **78**, 2775 (2001)

Size separation of carbon nanotubes for biomedical applications

Yoshinori Sato[a], Yuki Akimoto[a], Balachandran Jeyadevan[a], Kenichi Motomiya[b], Rikizo Hatakeyama[b], Kazuchika Tamura[c], Tsukasa Akasaka[c], Motohiro Uo[c], Atsuro Yokoyama[c], Ken-ichiro Shibata[c], Fumio Watari[c], Kazuyuki Tohji*[a]
[a]Graduate School of Environmental Studies, Tohoku University, Sendai, 980-8579, Japan
[b]Graduate School of Engineering, Tohoku University, Sendai, 980-8579, Japan
[c]Graduate School of Dental Medicine, Hokkaido University, Sapporo, 060-8586, Japan

ABSTRACT

In this paper, we report the results of an attempt to disperse MWCNTs in water and determine their biocompatibilities. The length of the MWCNTs was reduced by treating the acidic nanotube suspension with ultrasonic irradiation. Then, the cut nanotubes were size-separated into 670, 550 and 220 nm length by filtration using polycarbonate membrane filters. The neutrophils activity (TNF-α) of size-separated MWCNTs was low and confirmed biocompatible.

Keywords: Multi-walled carbon nanotubes (MWCNTs), size separation, biocompatibility, neutrophils activity, TNF-α

1. INTRODUCION

One of the challenging and exciting research areas is currently related to the bioactivity of carbon nanomaterials and their derivatives that have nano-spaces and large surface areas. Recently, carbon nanotubes (CNTs)[1-3] have been proposed for biomedical applications[4-9]. However, water-solubilization of the CNTs is indispensable for biomedical fields. Since the CNTs have chemical properties similar to graphite and are several micrometers long, they do not easily disperse in water on their own. Though the solubilization can be improved with the use of surfactants, it may affect the intracellular reactions and also complex reaction-phenomena on the physiological cells and tissues[10]. Thus, techniques to make aqueous dispersions of CNTs without the use of surfactants are desirable. Also, prior to the application of these dispersions in biomedical fields, the assessment of the potential health hazard of water-soluble CNTs for humans is important[11-15]. Here, we report the findings of a study carried out to disperse multi-walled carbon nanotubes (MWCNTs) in water by reducing the length of purified nanotubes by ultrasonicating the tubes in a an acidic medium, size-separate by the membrane filtration and their biocompatibilities by *in vitro* using human neutrophils of tumor necrosis factor-alpha (TNF-α).

2. EXPERIMENTAL DETAILS

2.1 Preparation of the size-separated MWCNTs

Purification procedure of MWCNTs. The MWCNTs synthesized by the CVD method and supplied by NanoLab was used in this study. The purity is 80 wt % with impurities such as amorphous carbon, Fe, Mo, Cr, Ni, and Al. The diameter is 20 – 40 nm, and the length is 5.0 μm on the average. First, MWCNTs were burned at 773 K for 90 min under atmospheric pressure. Then, the burned product was transferred into a flask with 1.0 L of 6M-HCl and treated at 333 K for 12 hours to remove the metals or metal oxides. Following this, the acid solution was filtered using a PTFE membrane filter with 0.1 μm pore size. The filtered cake was transferred into a flask with 1.0 L of 3M-NaOH and refluxed at 373 K for 15 hours to dissolve Aluminum oxides. The nanotubes are then recovered by filtering the suspension by using a membrane filter with 0.1 μm pore size, and the filtered cake was rinsed out with hot water. Finally, the sample was dried up at 333 K for 12 hours.

Cutting procedure of the purified MWCNTs. The cutting procedure of the purified MWCNTs is as follows: 100 mg of the purified MWCNTs was suspended in 100 mL of a 3:1 (v/v%) mixture of concentrated H_2SO_4 (95%) / HNO_3 (60%) and exposed to ultrasonic irradiation for 5 hours[16]. The acid-treated MWCNTs were filtered using a membrane filter with a pore size of 0.1 μm, and the filtered cake was rinsed out with water until the pH of filtrate becomes neutral.

Nanosensing: Materials and Devices, edited by M. Saif Islam, Achyut K. Dutta,
Proceedings of SPIE Vol. 5593 (SPIE, Bellingham, WA, 2004)
0277-786X/04/$15 · doi: 10.1117/12.579714

Size separation procedure of the cut MWCNTs. The size separation procedure of the cut MWCNTs is as follows[17]: 20 mg of the cut MWCNTs was suspended in 400 mL of ethanol and irradiated by ultrasonic for 1 hour. Next, the suspension was centrifuged at 5000 *g* for 1 hour in order to remove the aggregation of a few microns long MWCNTs and then the supernatant was filtrated using polycarborbonate membranes with cylindrical pore diameters 1.2, 0.8, and 0.4 μm.

Characterization of the purified and cut MWCNTs. The purified and cut MWCNTs were characterized with scanning electron microscope (SEM), transmission electron microscope (TEM), X-ray fluorescence spectroscopy (XRF), and Fourier transform infrared spectroscopy (FT-IR).

2.2 Biocompatibility test of the size-separated MWCNTs

Size-separated MWCNTs. Highly pure size-separated MWCNTs of 670, 550 and 220 nm were mixed with HBSS (Hanks' balanced salt solution) in concentrations of 0.5 μg/ml.

Cells used for toxicity test. Human peripheral blood was obtained from healthy volunteers in our group. Neutrophils were separated from blood using 6% isotonic sodium chloride containing hydroxyethyl starch and lymphocyte isolation solution. After the suspended size-separated MWCNTs solution was kept at 310 K for 2 weeks, neutrophils were added and incubated at 310 K for 30 min.

Cytokines (TNF-α). Tumor necrosis factor-alpha (TNF-α) production per 10^6 neutrophils in the supernatant was measured using ELISA kits.

3. RESULTS AND DISCUSSION

Figure 1 shows the SEM images of the raw (a), the purified MWCNTs (b) and the HRTEM image of the purified

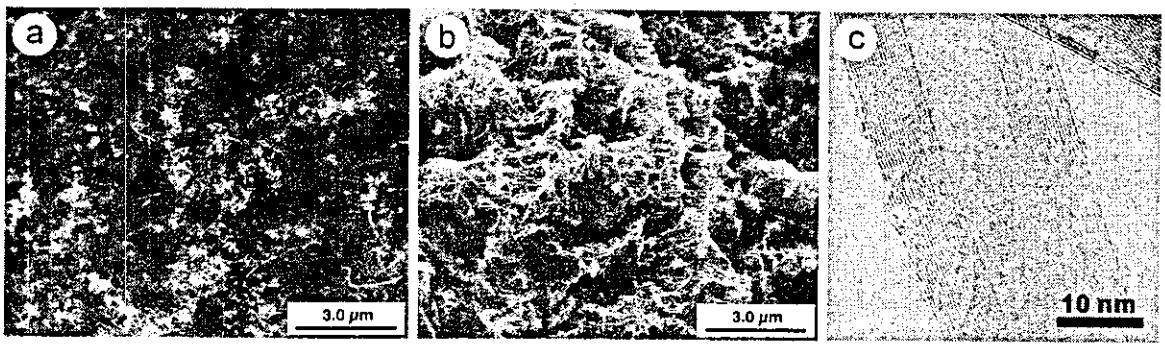

Figure 1. SEM images of the raw MWCNTs (a) and the purified MWCNTs (b). High magnification TEM image of the purified MWCNTs (c).

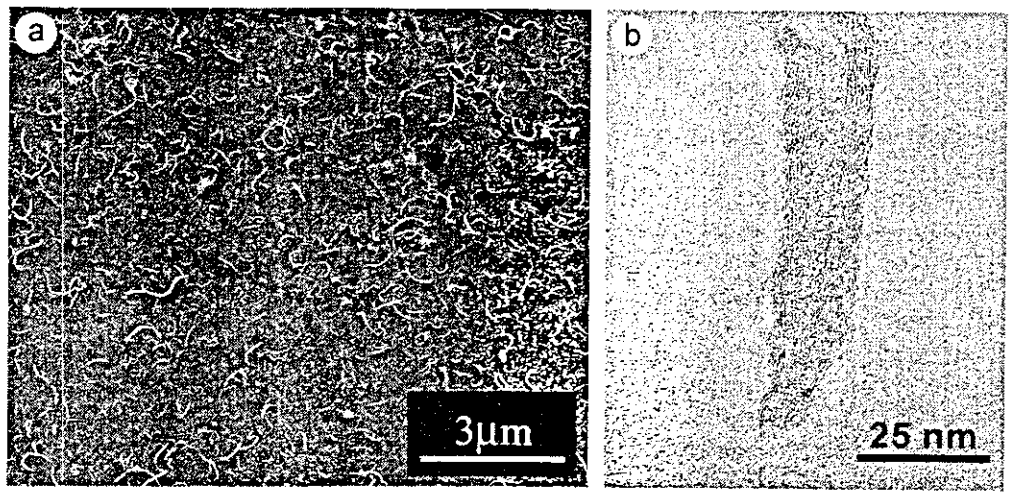

Figure 2. SEM and TEM images of the cut MWCNTs treated by the strong acids.

MWCNTs (c). It is clear from the SEM images that the purified MWCNTs were totally free of amorous carbon and carbon nanoparticles. The purified MWCNTs were confirmed to be free of metal impurities from TEM-EDX and XRF analyses. Furthermore, clear (002) lattice image of the purified MWCNTs (Figure 1c) suggested their highly crystalline nature. However, these tubes consist of many bamboo-like structures[18], and the diameter and length are not uniform in size.

Figure 2 shows the SEM (a) and TEM (b) images of the cut MWCNTs treated by the strong acids. It is obvious from the SEM image (Figure 2a) that the MWCNTs have been shortened and there is a large population of nanotubes that are less than 1.0 μm long. The cut nanotubes dispersed easily in the polar solvents such as ethanol and water. This may have become possible due to the reduced length and surface modification by the hydrophilic groups of the nanotube. However, the strong acid damaged the outer wall of MWCNTs, and the carbon network of MWCNTs was broken. However, the inner walls are intact. We believe that the property of the MWCNTs is retained.

We measured the FT-IR spectra of the cut MWCNTs in order to confirm the presence of the carboxyl and the hydroxyl groups (Figure 3). The IR spectrum of the cut MWCNTs has several peaks. The band between 1000 and 1200 cm^{-1} corresponds to stretching vibration of C-O and deformation vibration of OH. These bands are characterized by a shift to lower wavenumbers when a dimmer carboxyl is formed by hydrogen bonding[19]. The stretching vibration of aromatic C=C is observed between 1500 and 1600 cm^{-1}. On the other hand, the band between 2700 and 2900 cm^{-1} corresponds to the stretching vibration of CH attached to graphene edge. Also, the band around 3450 cm^{-1} is characteristic of the stretching vibration of OH and water. Thus, the surface of cut MWCNTs are modified by the carboxyl and hydroxyl functional groups and has made the dispersion of the same in water possible.

Figure 4 shows the SEM images (left) and their corresponding size-distribution (right) of the size-separated MWCNTs. The length of the nanotube becomes small, as the pore diameter of membrane filter is gradually decreased (Figure 4). The yield of MWCNTs with the average length of 220 nm (Figure 4c) was high compared with 670 and 550 nm (Figure 4a,b) length MWCNTs. These results demonstrate that we have been successful in isolating the cut nanotubes with average lengths 670, 550 and 220 nm. The IR analysis of the size–separated nanotube suggested that the surface structure depends on the length.

Figure 5 shows the amount of TNF-α released from neutrophils in HBSS containing size-separated nanotubes. For comparison, the amount of TNF-α released from neutrophils in HBSS containing Ti particles is plotted in the same graph[20]. In the case of Ti particles, TNF-α is released for particles with diameter less than 2.0 μm. Concerning the

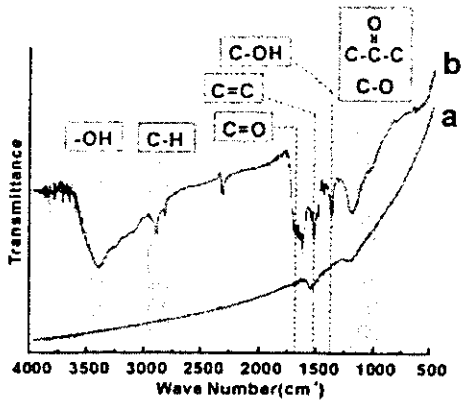

Figure 3. IR spectra of the purified MWCNTs (a) and the cut MWCNTs (b).

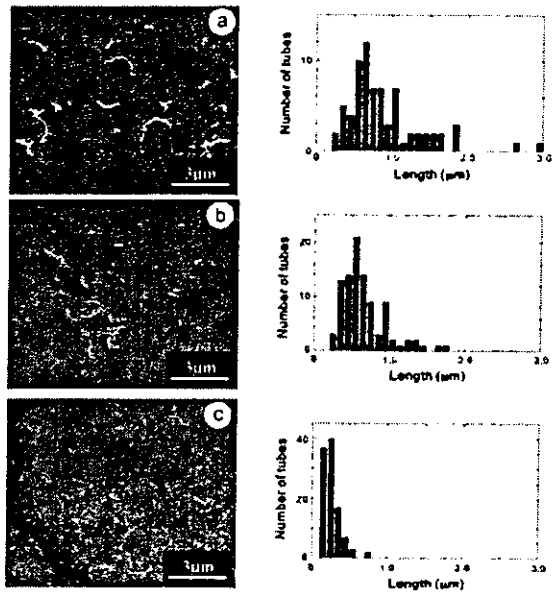

Figure 4. SEM images (left, a, b, c) and size-distribution (right) of the size-separated MWCNTs.

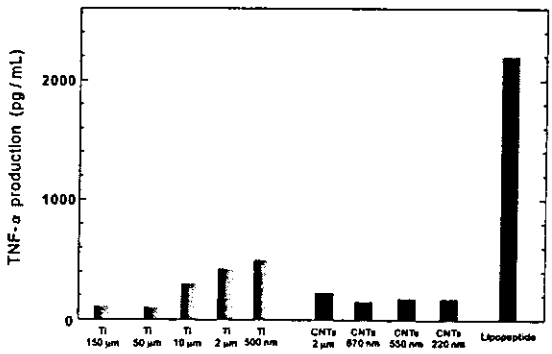

Figure 5. The amount of TNF-α released from neutrophils in HBSS containing size-separated nanotube and Ti particles.

relationship between cell and particle size on cytotoxicity, this effect is pronounced and the neutrophils activity increased[20] when the particles are smaller than the cell size. On the other hand, neutrophils activity is very low and their intensity does not depend on their size in the case of size-separated nanotubes shorter than 1.0 μm. Thus from our study, we could conclude that the carbon nanotube are highly biocompatibility. However, additional tests should be carried out to confirm the same.

4. CONCLUSION

We have succeeded in preparing highly pure size-separated MWCNTs. The biocompatibility test based on the neutrophils activity was carried out on these size-separated MWCNTs and proven to be non-toxic. The results of this study could be used to develop carbon-based materials for biomedical applications.

ACKNOWLEDGMENTS

This work was supported by Grant-in-Aid for Basic Research #(S) 14103016, and #(S) 13852016 from the Ministry of Education, Science, Culture and Sport of Japan and #H14-nano-021 from the Ministry of Health, Labor and Welfare.

REFERENCES

1. S. Iijima, "Helical Microtubules of Graphitic Carbon", *Nature*, **354**, 56-58, 1991.
2. S. Iijima and T. Ichihashi, "Single-Shell Carbon Nanotubes of 1-nm Diameter", *Nature* **363**, 603-605, 1993.
3. D. S. Bethune, C. H. Kiang, M. S. de Vries, G. Gorman, R. Savoy, J. Vazquez and R. Beyers, "Cobalt-Catalyzed Growth of Carbon Nanotubes with Single-Atomic-Layerwalls", *Nature* **363**, 605-607, 1993.
4. F. Belavoine, P. Schultz, C. Richard, V. Mallouh, T. W. Ebbesen and C. Mioskowski, "Helical Crystallization of Proteins on Carbon Nanotubes: A Fisrt Step toward the Development of New Biosensors", *Angew. Chem. Int. Ed.*, **38**, 1912-1915, 1999.
5. M. P. Mattson, R. C. Haddon and A. M. Rao, "Molecular Functionalization of Carbon Nanotubes and Use as Substrates for Neuronal Growth", *J. Mol. Neurosci.*, **14**, 175-182, 2000.
6. P. R. Supronowicz, P. M. Ajayan, K. R. Ullmann, B. P. Arulanandam, D. W. Metzger and R. Bisios, "Novel current-conducting composite substrates for exposing osteoblasts to alternating current stimulation", *J. Biomed. Mater. Res.*, **59**, 499-506, 2002.
7. A. Bianco and M. Prato, "Can Carbonnanotubes Be Considered Useful Tools for Biological Applications?", *Adv. Mater.*, **15**, 1765-1768, 2003.
8. D. Pantarotto, J. -P. Briand, M. Prato and A. Bianco, "Translocation of Bioactive Peptides across Cell Membranes by Carbon Nanotubes", *Chem. Comm.*, 16-17, 2004.
9. H. Hu, Y. Ni, V. Montana, R. C. Haddon and V. Parpura, "Chemically Functionalized Carbon Nanotubes as Substrates for Neuronal Growth", *Nano. Lett.*, **4**, 507-511, 2004.
10. R. Bandyopadhyaya, E. Nativ-Roth, O. Regev and R. Yerushalmi-Rozen, "Stabilization of Individual Carbon Nanotubes in Aqueous Solutions", *Nano Lett.*, **2**, 25-28, 2002.
11. V. L. Colvin, "The Potential Environmental impact of Engineered Nanomaterials", *Nat. Biotechnol.*, **21**, 1166-1170, 2003.
12. D. B. Warheit, B. R. Laurence, K. L. Reed, D. H. Roach, G. A. M. Reynolds and T. R. Webb, "Comparative Pulmonary Toxicity Assessment of Single-Wall Carbon Nanotubes in Rats", *Toxicol. Sci.*, **77**, 117-125, 2004.
13. C. –W. Lam, J. T. James, R. McCluskey and R. L. Hunter, D. B. Warheit, B. R. Laurence, K. L. Reed, D. H. Roach, G. A. M. Reynolds and T. R. Webb, "Comparative Pulmonary Toxicity Assessment of Single-Wall Carbon Nanotubes in Rats", "Pulmonary Toxicity of Single-Wall Carbon Nanotubes in Mice 7 and 90 Days after Intratracheal Instillation", *Toxicol. Sci.*, **77**, 126-134, 2004.
14. P. H. M. Hoet, A. Nemmar and B. Nemery, "Health Impact of Nanomaterials?", *Nat. Biotechnol.*, **22**, 19, 2004.
15. R. F. Service, "Nanomaterials Show Signs of Toxicity", *Science*, **300**, 243, 2003.
16. J. Liu, A. G. Rinzler, H. Dai, J. H. Hafner, R. K. Bradley, P. J. Boul, A. Lu, T. Iverson, K. Shelimov, C. B. Huffman, F. Rodriguez-Macias, Y. –S. Shon, T. R. Lee, D. T. Colbert and R. E. Smalley, "Fullerene Pipes", *Science*, **280**, 1253-1256, 1998.

17. T. Abatemarco, J. Stickel, J. Belfort, B. P. Frank, P. M. Ajayan and G. Belfort, "Fractionation of Multiwalled Carbon Nanotubes by Cascade Membrane Midrofiltration", *J. Phys. Chem.*, **103**, 3534-3538, 1999.
18. C. J. Lee, J. H. Park and J. Park, "Synthesis of Bamboo-shaped Multiwalled Carbon Nanotubes using Thermal Chemical Vapor Deposition", *Chem. Phys. Lett.*, **323**, 560-565, 2000.
19. H. –U. Gremlich and B. Yan, *Infrared and Raman Spectroscopy of Biological Materials*, Marcel Dekker, New York, 2002.
20. K. Tamura, N. Takashi, R. Kumazawa, F. Watari and Y. Totsuka, "Effects of Particle Size on Cell Function and Morphology in Titanium and Nickel", *Mater. Trans.*, **43**, 3052-3057, 2002.

*tohji@mail.kankyo.tohoku.ac.jp; phone +81 22 217 7390; fax +81 22 217 7390

Biocompatibility of carbon nanotube disk

Yoshinori Sato*[a], Makoto Ohtsubo[a], Balachandran Jeyadevan[a], Kazuyuki Tohji[a], Kenichi Motomiya[b], Rikizo Hatakeyama[b], Go Yamamoto[c], Mamoru Omori[c], Toshiyuki Hashida[c], Kazuchika Tamura[d], Tsukasa Akasaka[d], Motohiro Uo[d], Atsuro Yokoyama[d], Fumio Watari[d]
[a]Graduate School of Environmental Studies, Tohoku University, Sendai, 980-8579, Japan
[b]Graduate School of Engineering, Tohoku University, Sendai, 980-8579, Japan
[c]Fracture and Reliability Research Institute, Tohoku University, Sendai, 980-8579, Japan
[d]Graduate School of Dental Medicine, Hokkaido University, Sapporo, 060-8586, Japan

ABSTRACT

We report the preparation, properties and biocompatibility of multi-walled carbon nanotube (MWCNT) disk. Sintered Multi-walled carbon nanotube disk was fabricated by spark plasma sintering the MWCNT and phenol resin mixture by using the Spark Plasma System (SPS) under 1273 K and 80 MPa in vacuum. As the concentration of phenol resin in the sintered MWCNT disk increases, the bending strength and Young's modulus increased. However, the inflammatory response was observed in the tissue exposed to the surface of the sintered MWCNT disk. This was believed due to the residual phenol resin in the disk. The result indicates that the disk has to be annealed at higher temperatures under inert gas atmosphere to perfectly convert phenol resin to graphitic materials.

Keywords: Multi-walled carbon nanotubes (MWCNTs), spark plasma system (SPS), inflammatory response, biocompatibility, fibrous connective tissue, lymphocyte

1. INTRODUCION

Carbon composites have been proposed as an alternate biomaterial for dental and internal organ that require high bending strength with lightweight. Until now, C/C (carbon-carbon) composites have been considered for artificial heart valves[1, 2] and tooth roots[3]. However, the mechanical strength has not been high enough. On the other hand, carbon nanotubes (CNTs)[4-6] and their composites[7-10] and fibers[11-16] have been proposed to be used in the field of aerospace technology because the CNTs have unique mechanical properties such as 0.3-1.0 TPa of high Young's modulus and 11-200 GPa of tensile strength[17]. We believe that the carbon nanotubes have potential to replace the traditional biomaterials. Here, we report the preparation, mechanical properties and biocompatibility of the sintered multi-walled carbon nanotube disk.

2. EXPERIMENTAL DETAILS

2.1 Materials and characterization

Purification of MWCNTs. We used the MWCNTs synthesized by the CVD method (NanoLab Inc., US, 80 wt% purity). The impurities were amorphous carbon, Fe, Mo, Cr, Ni, and Al. The diameter lies between 20 and 40 nm, and the average length is 5.0 μm. First, MWCNTs were burned at 773 K for 90 min under atmospheric pressure. The burned product was then transferred into a flask with 1.0 L of 6M-HCl and treated at 333 K for 12 hours to remove the metals or metal oxides except aluminum oxide. Following this, the suspension was filtered using a PTFE membrane with the pore size of 0.1μm. The filtered cake was transferred into a flask with 1.0 L of 2M-NaOH and refluxed at 373 K for 15 hours to dissolve aluminum oxides. The suspension was then filtered using a membrane filter (PTFE membrane with the pore size of 0.1μm) and the filtered cake was washed. Finally, the sample was dried at 333 K for 12 hours. The structure of the sintered MWCNT disk was

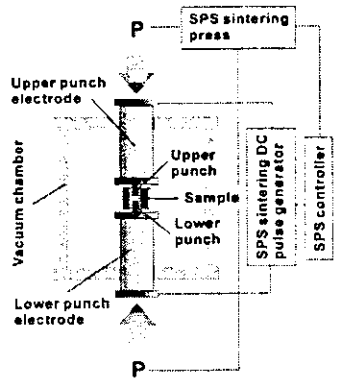

Figure 1. Illustration of Spark Plasma System (SPS).

Nanosensing: Materials and Devices, edited by M. Saif Islam, Achyut K. Dutta,
Proceedings of SPIE Vol. 5593 (SPIE, Bellingham, WA, 2004)
0277-786X/04/$15 · doi: 10.1117/12.579687

characterized with scanning electron microscope (SEM), transmission electron microscope (TEM), X-ray fluorescence spectroscopy (XRF), and Fourier transform infrared spectroscopy (FT-IR).

Preparation of MWCNT disk. Sintered Multi-walled carbon nanotube disk was fabricated by spark plasma sintering the MWCNT and phenol resin mix by using the spark plasma system (SPS) under 1273 K and 80 MPa in vacuum for 1 hour. The SPS has been developed for sintering of metal and ceramics in the plasma and electric field, and it is used for consolidation of various kinds of materials such as metals, ceramics and polymer[18, 19]. This system consists of vacuum chamber, punch electrodes, graphite die, SPS DC-pulse power generator, SPS sintering press, and SPS controller (Figure 1). The nanotube powders were put in a graphite die with 10 mm diameter hole and set in the SPS. The mechanical property of the MWCNT disk was measured by using a small punch test (SP). The SP equipment consists of the puncher, upper and lower die. The specimen (MWCNT disk) is subjected to a puncher driven at a constant displacement rate through the guide hole, and the puncher force and displacement were recorded.

2.2 Biocompatibility test of the sintered MWCNT disk

A rectangular parallelepiped MWCNT of 1.5 x 1.5 x 5.0 mm in size was used as an implant material. The sample was implanted in the subcutaneous connective tissue in the abdominal region of Wistar strain rats. After the rats were anesthetized with diethyl ether, pentobarbital sodium was injected into the abdominal cavity of the rats and the metal implants were inserted in the subcutaneous connective tissue in the abdominal region of the rats to observe the response of soft tissue. After one week, the MWCNT disk implanted in the subcutaneous tissue was carefully removed from the resected tissue block after fixation in 10% neutral buffered formalin, and the tissue block was embedded in paraffin by the conventional method. The tissue block was sectioned and stained with hematoxylin-eosin [20,21]. These specimens were observed with an optical microscope. When inflammatory response arises, fibrous connective tissue becomes thick and lymphocyte is observed in the fibrous connective tissue.

3. RESULTS AND DISCUSSION

Figure 2a shows the SEM image of the purified MWCNTs. It is clear that the purified MWCNTs were totally free of amorphous carbon and carbon nanoparticles. These tubes consist of many bamboo-like structures (Figure 2b), and the diameter and length are not uniform in size. The phenol resin and the purified MWCNTs were dispersed into ethanol and sonicated for 1 hour. The amount of phenol resin in the MWCNT-phenol resin mixture was fixed at 25 and 50 wt%. Next, the ethanol was evaporated at 343 K under atmospheric pressure, and the mixtures were heated at 573 K for 1 hour under N_2 atmosphere to convert the phenol resin into carbon materials.

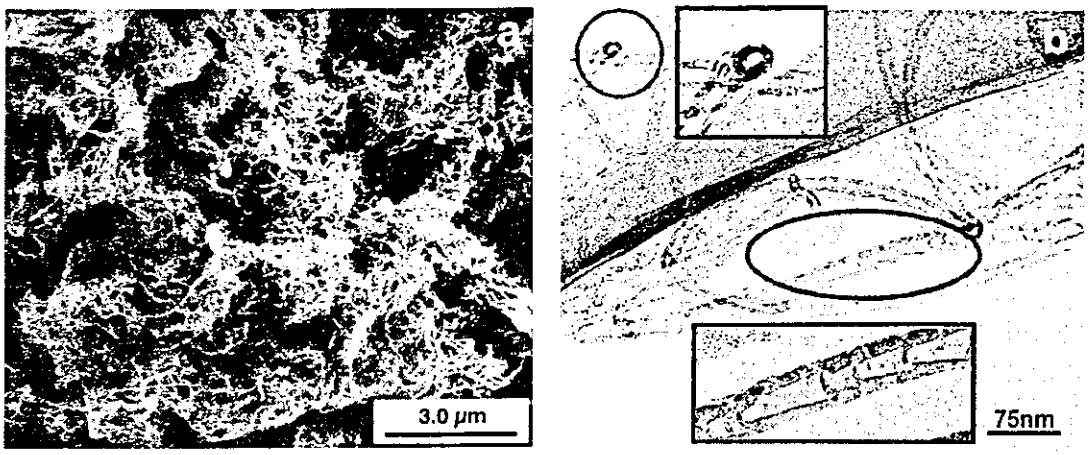

Figure 2. SEM image of the purified MWCNTs (a) and TEM image of the MWCNTs with bamboo-like structure (b).

Figure 3 shows the SEM image of MWCNTs in the MWCNT-phenol resin mixture with 50 wt% phenol resin. The arrows in Figure 3 indicate the areas of decomposed phenol resins. Figure 4 is the photograph of the sintered MWCNT disk with 10 mm in diameter and 1.5 mm in thick. The MWCNT disk that could withstand the mechanical test (SP) was prepared successfully. Table 1 shows the bending strength, Young's modulus and apparent density of the

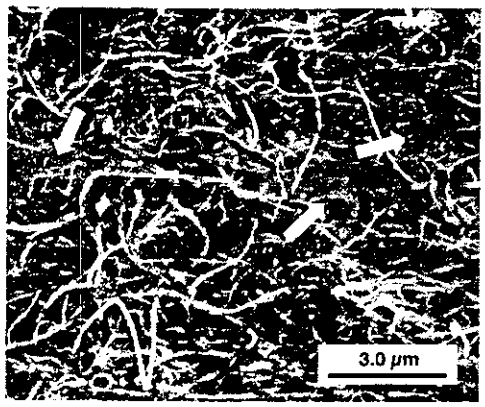

Figure 3. SEM image of MWCNTs with 50 wt% phenol resin. Arrows are the decomposed phenol resins.

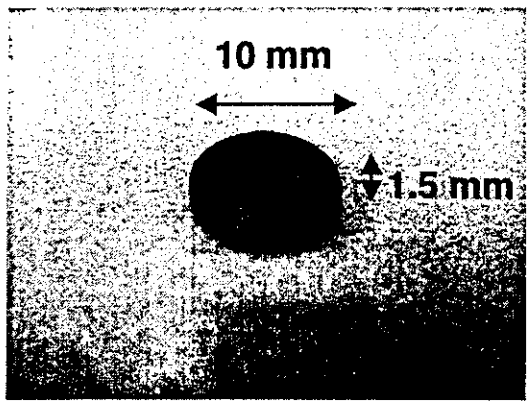

Figure 4. The photograph of the sintered MWCNTs disk produced by SPS.

sintered MWCNT disk. The mechanical properties determined from the SP test of the MWCNT disk prepared with 25 wt% phenol resin, were 72.7 MPa (bending strength), 1.5 GPa (Young's modulus), and 1.38 g/cm^3 (apparent density). On the other hand, the mechanical properties of the MWCNT disk prepared with 50 wt% phenol resin were determined to be 91.4 MPa (bending strength), 2.3 GPa (Young's modulus), and 1.41 g/cm^3 (apparent density). Our results clearly indicate that the mechanical strength is improved when the amount of phenol resin in the MWCNT-phenol resin mixture was increased. However, the recorded mechanical properties were not high enough in comparison with the human bone[2]. The reason for the low value can be either due to weak bonding between tubes or binder and the tube

Table 1. Mechanical properties and apparent density of the sintered MWCNT disk.

Material	Bending strength (MPa)	Young's modulus (GPa)	Apparent density (g/cm^3)
MWCNTs disk with 25 wt%	72.2	1.53	1.38
MWCNTs disk with 50 wt%	91.4	2.36	1.41
Human bone	150	16-18	—

Figure 5 shows the optical micrographs of the tissue response to the sintered MWCNT disk with 50 wt. % phenol resin in the subcutaneous tissue of rat after one week. Figure 5b is the higher magnification optical micrograph of the rectangle frame shown in the figure 5a. The sintered MWCNT disk implants were encapsulated with thick fibrous connective tissue, with some lymphocytes (circled in Figure 5b). This tendency was also observed in the sintered MWCNT disk with 25 wt % phenol resin. These results are an indication of inflammatory response. On the other hand, in case of the C/C composite implants, the fibrous connective tissue is thin and no inflammatory response was observed. Thus, the sintered MWCNT disk prepared with phenol resin as binder is believed to be less biocompatible. One of the reasons for the inflammatory response is due to the residue of undecomposed phenol resin in the sintered MWCNT disk.

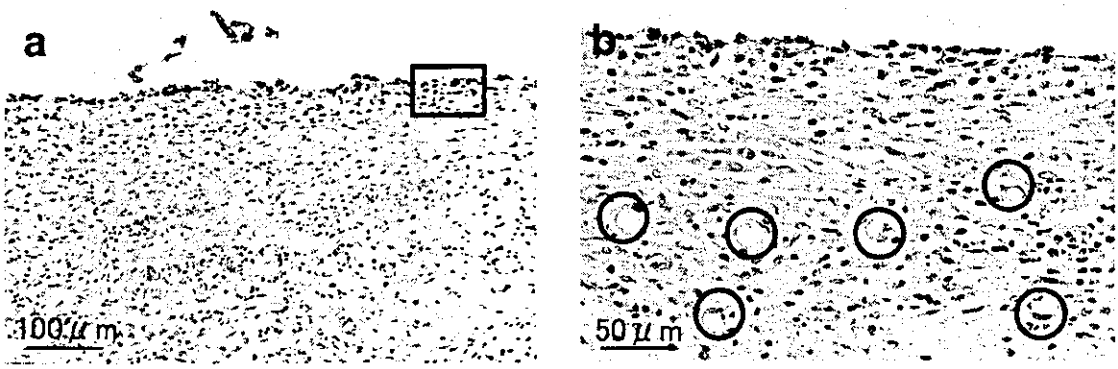

Figure 5. Optical micrographs of the tissue response to the sintered MWCNT disk mixed with 50 wt% in the subcutaneous tissue of rat after one week. Figure 5b is the high magnification optical micrograph of a squire frame in the Figure 5a. Lymphocytes are in open circles.

4. CONCLUSION

Sintered multi-walled carbon nanotube disk was produced by SPS under the condition of 1273 K at 80 MPa in vacuum. As the concentration of the phenol resin is increased in the sintered MWCNT disk, the bending strength and Young's modulus increased. However, the recorded mechanical properties were not high enough to consider it as an alternative to human bone. Though the mechanical properties were improved with higher phenol resin concentration, the inflammatory response was observed in the tissue exposed to the surface of the sintered MWCNT disk. The inflammatory response is the residue of undecomposed phenol resin in the sintered MWCNT disk. In order to improve the biocompatibility of sintered MWCNT disk, the disk has to be annealed at higher temperatures under inert gas atmosphere to totally convert phenol resin to graphite.

ACKNOWLEDGMENTS

This work was supported by Grant-in-Aid for Basic Research #(S) 14103016, and #(S) 13852016 from the Ministry of Education, Science, Culture and Sport of Japan and #H14-nano-021 from the Ministry of Health, Labor and Welfare.

REFERENCES

1. J. C. Bokros, "Carbon Biomedical Devices", *Carbon*, **15**, 353-371, 1977.
2. A. D. Haubold, H. S. Shim, J. C. Bokros, "Developments in Carbon Prosthetics", *Biomaterials Medical Devices and Artificial Organs*, 7, 263-269, 1979.
3. G. M. Jenkins, "Biomedical Applications of Carbon-Fiber Reinforced Carbon in Implanted Prostheses", *Carbon*, **15**, 33-37, 1977.
4. S. Iijima, "Helical Microtubules of Graphitic Carbon", *Nature*, **354**, 56-58, 1991.
5. S. Iijima and T. Ichihashi, "Single-Shell Carbon Nanotubes of 1-nm Diameter", *Nature* **363**, 603-605, 1993.
6. D. S. Bethune, C. H. Kiang, M. S. de Vries, G. Gorman, R. Savoy, J. Vazquez and R. Beyers, "Cobalt-Catalyzed Growth of Carbon Nanotubes with Single-Atomic-Layerwalls", *Nature* **363**, 605-607, 1993.
7. L. S. Schadler, S. C. Giannaris and P. M. Ajayan, "Load Transfer in Carbon Nanotube Epoxy Composites", Appl. Phys. Lett., 73, 3842-3844, 1998.
8. A. A. Mamedov, N. A. Kotov, M. Prato, D. M. Guldi, J. P. Wicksted and A. Hirsch, "Molecular Design of Strong Single-Wall Carbon Nanotubes/Polyelectrolyte Multilayer Composites", *Nature Mater.*, **1**, 190-194, 2002.
9. G. –D. Zhan, J. D. Kuntz, J. Wan and A. K. Mukherjee, "Single-Wall Carbon Nanotubes as Attractive Toughening Agents in Alumina-based Nnaocomposites", *Nature Mater.*, **2**, 38-42, 2003.
10. X. Wang, N. P. Padture and H. Tanaka, "Contact-Damage-Resistant Ceramic/Single-Wall Carbon Nanotubes and Ceramic/Graphite Composites", *Nature Mater.*, **3**, 539-544, 2004.

11. R. Andrews, D. Jacques, A. M. Rao, T. Rantell, F. Derbyshire, Y. Chen, J. Chen and R. C. Haddon, "Nanotube Composite Carbon Fibers", *Appl. Phys. Lett.*, **75**, 1329-1331, 1999.
12. B. Vigolo, A. Pénicaud, C. Coulon, C. Sauder, R. Pailler, C. Journet, P. Bernier and P. Poulin, "Macroscopic Fibers and Ribbons of Oriented Carbon Nanotubes", *Science* **290**, 1331-1334, 2000.
13. H. W. Zhu, C. L. Xu, D. H. Wu, B. Q. Wei, R. Vajtai, P. M. Ajayan, "Direct Synthesis of Long Single-Walled Carbon Nanotubes Strands", *Science* **296**, 884-886, 2002.
14. A. B. Dalton, S. Collins, E. Muñoz, J. M. Razal, V. H. Ebron, J. P. Ferraris, J. N. Coleman, B. G. Kim and R. H. Baughman, "Super-Tough Carbon-Nanotube fibres", *Nature* **423**, 703 (2003).
15. Y. –Li. Li, I. A. Kinloch and A. H. Windle, "Direct Spinning of Carbon Nanotubes Fibers from Chemical Vapor Deposition Synthesis", *Science* **304**, 276-278, 2004.
16. L. M. Ericson, H. Fan, H. Peng, V. A. Davis, W. Zhou, J. Sulpizio, Y. Wang, R. Booker, J. Vavro, C. Guthy, A. N. G. Parra-Vasquez, M. J. Kim, S. Ramesh, R. K. Saini, C. Kittrell, G. Lavin, H. Schmidt, W. W. Adams, W. E. Billups, M. Pasquali, W. –F. Hwang, R. H. Hauge, J. E. Fischer and R. E. Smalley, "Macroscopic, Neat, Single-Walled Carbon Nanotubes Fibers", *Science* **305**, 1447-1450, 2004.
17. M. –F. Yu, B. S. Files, S. Arepalli and R. S. Ruoff, "Tensile Loading of Ropes of Single Wall Carbon Nanotubes and their Mechanical Properties", *Phys. Rev. Lett.*, **84**, 5552-5555, 2000.
18. M. Omori, "Sintering, Consolidation, Reaction and Crystal Growth by the Spark Plasma System (SPS)", *Mater. Sci. Eng. A*, **287**, 183-188, 2000.
19. M. Omori, A. Okubo, M. Otsubo, T. Hashida and K. Tohji, "Consolidation of Multi-Walled Carbon Nanotube and Hydroxyapatite Coating by the Spark Plasma System (SPS)", *Key Eng. Mater.*, **254-256**, 395398, 2004.
20. H. Matsuno, A. Yokoyama, F. Watari, M. Uo and T. Kawasaki, "Biocompatibility and Osteogenesis of refractory metal implants, titanium, hafnium, niobium, tantalum and rhenium", *Biomaterials*, **22**, 1253-1262, 2001.
21. A. Yokoyama, H. Matsuno, S. Yamamoto, T. Kawasaki, "Tissue Response to A Newly Developed Calcium Phosphate Cement Containing Succinic Acid and Carboxymethyl-Chitin", *J. Biomed. Mater. Res.*, **64A**, 491-501, 2003.

*hige@bucky1.kankyo.tohoku.ac.jp; phone +81 22 217 7392; fax +81 22 217 7392

PROCEEDINGS of 2nd International Workshop on WATER DYNAMICS
Tohoku University, Sendai, Japan, 11-12 November, 2004

Application of multi-walled carbon nanotubes to CdS photocatalytic system

Y.SAWADA[1], T.ARAI[2], Y.SATO[1], K.SHINODA[1], B.JEYADEVAN[1], K.TOHJI[1]

[1]Graduate School of Environmental Studies, Tohoku University, Sendai, Japan
[2]Institute of Fluid Science, Tohoku University, Sendai, Japan

ABSTRACT – Cadmium Sulfide (CdS) semiconductor particles that operate as a photocatalyst in the visible light region were deposited on the surface of modified multi-walled carbon nanotubes (MWCNTs) by chemical bath deposition (CBD) method. The enhancement of photocatalytic activity of CdS/MWCNTs was observed in the hydrogen generation experiment carried out using the visible light radiation and role of MWCNTs as an electrode was confirmed. Modifying the surfaces of MWCNTs with induced defects controlled the particle CdS size. The increase of specific surface area of CdS resulted in decreased amounts of hydrogen generated. Consequently, the photocatalytic activity of CdS/MWCNTs was strongly influenced by the state of the surface and electronic properties of MWCNTs.

1. INTRODUCTION

Recently, there has been considerable interest in hydrogen energy, which is believed to be the answer for the environmental problem faced by the mankind at present. From this point of view, the photocatalytic system that produces hydrogen with solar energy has been considered very promising. We have been successful in effectively splitting hydrogen sulfide molecule using Pt supported CdS photocatalyst with a specific morphology (stratified structure) in the visible light region[1]. Though the physical structure of the particle was very vital for the separation of the oxidation-reduction reaction sites, the photocatalytic efficiency of these particles strongly depended on Pt that acts as an electrode. As Pt is very costly, alternative material has to be considered for practical application.

Since the discovery of carbon nanotubes with unique properties in 1991[2], they have been considered for many applications. We believe that carbon nanotubes could be used as CdS photocatalyst support because of their size, chemical stability, and semiconductor properties. The deposition of CdS on MWCNTs may promote the formation of small particles and prevent particle aggregation.. Additionally, we desire to achieve the separation of oxidation-reduction reaction sites using the tubular structure and electric properties of the nanotubes.

In this paper, we report the effect of the surface of MWCNTs on their electronic state, and photoreactivity of CdS/MWCNTs.

2. EXPERIMENT

2.1 Preparation of surface modified MWCNTs

MWCNTs were synthesized by chemical vapor decomposition method using metal catalysts (NanoLab Inc.,). The as-grown samples were air-oxidated and acid treated to remove the metal catalysts. Then, these samples were treated to obtain MWCNTs with different surface properties for the deposition of CdS. Here, we prepared four types of samples for this study. First, the purified sample was treated with ozone to make the surface of the nanotubes have hydrophilic nature. Here, 100 mg of MWCNTs were dispersed in 300 ml of toluene using ultrasonication. Then, the suspension was bubbled with ozone gas for one hour. The ozonized sample was filtered and washed out with ethanol. This sample is named as 'sample A' Then, the sample B was prepared by annealing the purified nanotubes at 2273 K for 5 hours in high vacuum furnace and treated with ozone. The annealing treatment improved the crystallinity of the MWCNTs surface through the rearrangement of carbon atoms by thermal energy. And the ozone treatment was carried out to make the nanotube surface hydrophilic. Then, samples C and D were prepared from cut purified nanotubes. In the case of sample C, 100 mg of purified MWCNTs was added into 100 ml of mixed acid (conc.H_2SO_4 (95%): conc.NO_3 (60%) =75 ml : 25 ml) solution and ultrasonicated and stirred for 3 hours. This process facilitates the cutting and surface modification in a single step[3][4]. Then, the cut sample was annealed and ozonated under conditions stipulated in the preparation of sample B to obtain sample D.

All the samples were characterized by Raman spectroscopy (Jobin Yvon Spex; T64000), scanning electron microscope (SEM, Hitachi; 4100) and transmission electron microscope (TEM, Hitachi; HF-2000).

2.2 CdS deposition on MWCNTs

CdS was deposited by CBD method on MWCNTs samples (A)-(D). The deposition of CdS particles on MWCNTs were realized by introducing specified amount of MWCNTs into 100 ml of 0.01M $3CdSO_4 \cdot 8H_2O$, 1.0M NH_3, and 0.01M $SC(NH_2)_2$ mixed solution and heating to

358 K and allowed to cool down to room temperature in one hour . The reaction conditions, such as reaction time, temperature, and concentration of reagents were kept constant, but the amount of MWCNTs introduced was adjusted to maintain the surface area of the sample equal. CdS/MWCNTs were analyzed by SEM, TEM, and XRD.

2.3 Irradiation Experiment

Photocatalytic reactivities of the CdS/MWCNTs samples were evaluated by splitting the hydrogen sulfide molecule using the visible light irradiation. A specified amount of CdS/MWCNTs samples were introduced into 0.1M Na_2S solution. The hydrogen generation reaction from Na_2S solution was assumed to occur as follows:

$$Na_2S + H2O \rightarrow 2Na^+ + HS^- + OH^-$$

$$2H^+ + 2e^- \rightarrow H_2$$

$$2HS^- \rightarrow 2H^+ + S_2^{2-} + 2e^-$$

$$\Rightarrow 2HS^- \rightarrow H_2 + S_2^{2-}$$

Solar spectrum was simulated using Xenon Lamp (Wakomu-Denso: KXL-552HPF: 550W). The amount of hydrogen generated in 4 hours was recorded.

3. RESULT AND DISCUSSION

3.1 Preparation of MWCNTs

As shown in Fig.1, the MWCNTs were free of impurities and confirmed the effectiveness of the purification process. Then, the ozonized purified MWCNTs were dispersed well in distilled water

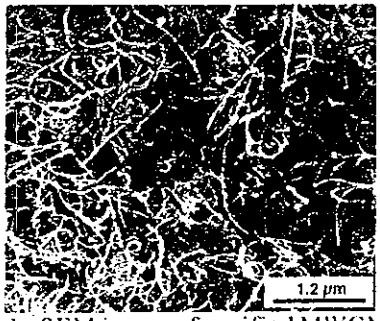

Fig1. SEM image of purified MWCNTs

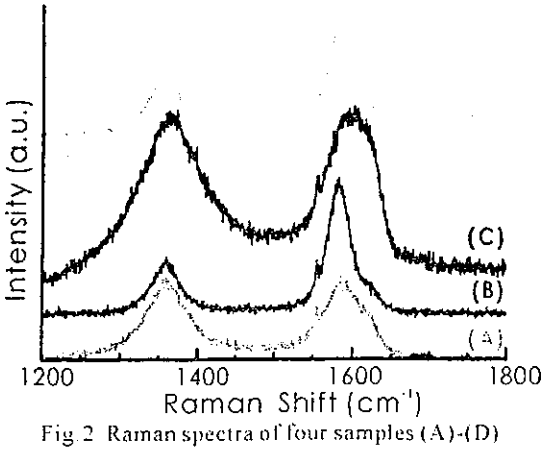

Fig.2 Raman spectra of four samples (A)-(D)

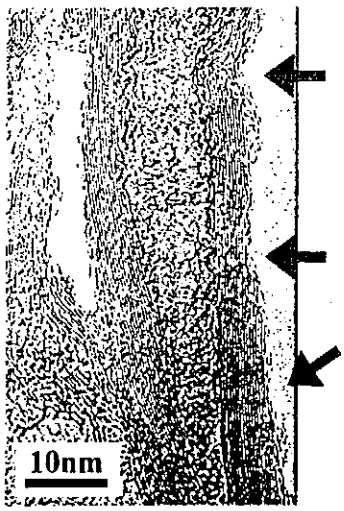

Fig.3 TEM image of cut MWCNTs (defects are indicated by arrows)

suggesting that the surface of the nanotubes has become hydrophilic. The hydrophilic nature of the surface is believed due to the presence of oxidized functional groups. The Raman spectrum of MWCNTs (Fig.2) showed the two main peaks centered at 1580 cm^{-1} and 1350 cm^{-1} derived from crystalline graphite (G-band) and defects or disordered crystalline graphite (D-band) respectively. We can discuss the crystallinity of MWCNTs by comparing the G and D band ratio (G/D). As shown in Fig.2, we observed the improvement of the same by annealing the samples at 2273 K for 5 hours in vacuum. The TEM micrograph of the cut sample is shown in Fig. 3. The surface roughness observed in Fig.3 was due to the defects created by the acid treatment. Cut nanotubes also exhibited affinity towards water as in the case of sample A. Table.1 shows the results of specific surface area of each sample measure by using the BET method. Though the specific surface area of oxidized MWCNTs is expected to increase[5][6], the cut and ozone treated samples showed a decrease in surface area. Presumably, strong oxidizing power of the mixed acid solution and ozone may have converted the graphite sheets into amorphous carbon. Furthermore, the specific surface area of annealed samples decreased significantly. This is believed due to clean, defect-free smoothed surfaces of the nanotubes.

	Purified MWCNTs	(A)	(B)	(C)	(D)
Specific Surface area (m^2/g)	246.6	241.2	146.3	209.3	155.9

Table1 Mesuring results of specific Surface area

3.2 Properties of CdS/MWCNTs

From the XRD patterns of the CdS/MWCNTs (Fig.4), the presence of cadmium compounds were identified and found to be that of cubic CdS and hexagonal cadmium hydroxide ($Cd(OH)_2$). As seen from the TEM photographs in Fig. 5, the particle sizes of the CdS deposited on the nanotubes differ. The UV-VIS spectra of the